NOTES AND CORRESPONDENCE

Oceanic Freshwater Budget and Transport as Derived from Satellite Radiometric Data

DIDIER JOURDAN,* PETER PETERSON, AND CATHERINE GAUTIER

Earth-Space Research Group, Institute for Computational Earth System Science, University of California, Santa Barbara, Santa Barbara, California

20 April 1995 and 1 January 1996

ABSTRACT

Blended satellite–ship evaporation and SSM/I retrieved precipitation fields are used to compute oceanic freshwater budget (FWB) and transport (FWT) over a 3-year period (1988–90). In order to validate the results, comparisons on monthly, seasonal, and multiyear average bases are performed with ECMWF analyzed field and climatology respectively. For May 1988, differences between ECMWF output and the present monthly estimate are within 2 mm day^{-1} (73 cm yr^{-1}). Comparison with climatology shows that global discrepancies for long-term average drop down to 36 cm yr^{-1} rms with a tendency for satellite-derived results to enhance climatological features. Differences are found to correlate with FWB patterns: large positive differences are observed in strong evaporative regions (eastern tropical Pacific), whereas negative differences are observed over the eastern part of the intertropical convergence zone and the northwestern part of the subtropical basins. Over the latter, precipitation is strongly dominant in our results, whereas climatology features rather slightly negative or positive contribution to the FWB (i.e., evaporation). Over the Gulf Stream, for example, climatology indicates that ocean is losing about 100 cm yr^{-1} freshwater while FWB is balanced in our computation. FWT is then computed and compared with climatological and in situ estimates. Differences with climatology are found to be 0.2 Sv rms (Sv $\equiv 10^6$ m^3 s^{-1}) in the Atlantic, Indian, and Northern Pacific Oceans, and results generally match estimates derived from oceanographic data within the same error level, except in the Indian Ocean. The major disagreement is observed in the southern Pacific Ocean where results, although confirming the direction of the FWT, suggest that 2.48 Sv is entering the Pacific Ocean, whereas climatologies only give a northward transport equal to 0.26 Sv.

1. Introduction

The oceanic freshwater budget (FWB) is defined as the difference between the sink, evaporation (E), and the sources, precipitation (P), and runoff (R) of freshwater in the ocean. It is not balanced everywhere at the surface, but globally precipitation and runoff compensate for the loss of freshwater due to the evaporation. The local unbalance in the FWB implies that seawater (freshwater and salt) is transported by oceanic circulation from regions where precipitation exceeds evaporation (net gain of freshwater by the ocean) to regions where evaporation process is dominant (net loss of freshwater). This can be defined as the net water transport (NWT).

Over a long enough time scale, the change in NWT is related to the divergence of FWB. In other words, the flux of freshwater lost by evaporation through the upper side $dx.dy$ of an elementary box in the ocean is replaced by the flux of seawater advected within the box through its lateral sides between the surface and the seafloor. Where the oceanic basins are bounded east and west, the NWT integrated over the basin width only has a meridional component given by

$$\mathrm{NWT}(y) = \iiint \rho v \, dx \, dz \, dt = \iiint [E - (P + R)] \, dx \, dy \, dt, \quad (1)$$

where v is the meridional velocity in the ocean and ρ the density of seawater. By convention, the NWT is defined positive northward.

Wijffels et al. (1992) showed that for global studies freshwater transport (FWT) has to be defined as the fraction of NWT that is pure, namely, $(1 - S)$ where S is the salinity, rather than based on the deviation to a reference salinity. This definition of FWT yields

*Current affiliation: Départment D'Océanographie Appliquée, EPSHOM/CMO, Brest, France.

Corresponding author address: Dr. Didier Jourdan, Dépt. D'Océanographie Appliquée, EPSHOM/CMO, 13 rue du Chatellier, B.P. 426, 29275 Brest Cedex, France.

$$\mathrm{FWT}(y) = \iiint (1 - S)\rho v \, dx \, dz \, dt$$
$$= \iiint \rho v \, dx \, dz \, dt - \iiint S\rho v \, dx \, dz \, dt. \quad (2)$$

Since salt is a conservative property of seawater, $\iiint S\rho v \, dx \, dz \, dt = 0$ and by substituting the right-hand term with Eq. (1), FWT is given by

$$\mathrm{FWT}(y) = \iiint [E - (P + R)] \, dx \, dy \, dt. \quad (3)$$

When FWT is known across a given latitude, the integration of the FWB gives FWT across any zonal section farther south in the ocean. It must be noted that the same computation gives the NWT [Eq. (1)] if the starting integration constant is chosen to be the mass transport through the section.

Over the continents, the FWB components are well monitored, but few estimates of E and P are available over the oceans. In the open ocean, the fields are computed from meteorological reports collected by ships and have inherent problems to shipboard measurements (Cardone 1990). Parameters are often inaccurate because the instruments are poorly maintained or wrongly operated. Differences in measuring method and the modification of the airflow and temperature around the ship structure cause errors. Also the sampling may be inadequate in some regions (Taylor 1984; Jourdan and Gautier 1995), and the oceanic freshwater flux at the surface is often estimated by extrapolating the measurements acquired in coastal and island regions across oceanic regions rarely visited. Baumgartner and Reichel (1975, hereafter BR) used this type of data, along with earlier results, to compute their global maps of E and P. Numerous studies rely on these estimates of the FWB components, either used both together to compute FWT (Baumgartner and Reichel 1975; Wijffels et al. 1992) or as a reference with to compare other FWT estimates (Schmitt et al. 1989).

FWT can also be computed from oceanographic measurements of wind, temperature, salinity, and ocean currents along oceanic sections (Hall and Bryden 1982; Toole and Raymer 1985). For convenience, FWT can be split up in three different components according to the process involved in the transport: Ekman forcing, western boundary current, and midocean geostrophic circulation. The Ekman transport is obtained from surface map of wind stress (Leetma and Bunker 1978; Hellerman and Rosenstein 1983). The flow in the western boundary current and in midocean region is separated into barotropic and baroclinic contribution: The baroclinic component can be calculated directly from the hydrographic station data in both circulation regimes. As for the barotropic component, it is usually well determined within the west boundary currents because of extensive experiments led in these regions but is poorly known in the midocean. Therefore, the method is based on the assumption that there is no net mass transport across the section and that the northward transport by the west boundary current is compensated by a southward circulation across the section elsewhere. This is the major limitation of the oceanographic based computation along with errors of in situ measurements. Indeed, time required to complete oceanographic sections and often low spatial resolution along them usually does not allow one to resolve the contribution of the mesoscale oceanic circulation. Also, the oceanographic data are limited in time and preclude estimation of the net impact of seasonal variations on the transport.

For all these reasons, the ocean–atmosphere exchange budget is often preferred to assess FWB. In this paper we will take advantage of the global and synoptic coverage provided by remote sensed observations to estimate the E and P components and to compute FWB and FWT over the global ocean. The next section briefly describes the E and P fields used and the method to compute FWT. In section 3, $E - P$ maps and meridional FWT results are compared with some earlier estimates based on both surface exchange and oceanographic computations. Section 4 discusses discrepancies and the situation in the southern Pacific Ocean where our results strongly differ from all the other estimates available.

2. Evaporation minus precipitation and FWT computation

a. Evaporation minus precipitation maps

1) EVAPORATION DATA

Evaporation is linked to latent heat flux (LHF) through the latent heat of vaporization. Thorough comparisons have been completed between satellite-derived and ship-based estimates of LHF (Esbensen et al. 1993; Jourdan and Gautier 1995). Results showed that the small number, or even the lack, of ship measurements in some oceanic areas explains the 40% random difference observed between both types of LHF computation (Jourdan and Gautier 1995). On the other hand, purely satellite-derived fields exhibit systematic errors in strong atmospheric subsidence regions and over oceanic upwelling regions due to the failure of the global relationships used to compute air mixing ratio and air temperature from remote sensed precipitable water (Esbensen et al. 1993).

To take advantage of the strength of both data types, Jourdan and Gautier (1995) combined satellite and ship derived LHF estimates. The idea that supported the blended analysis was to combine ship and satellite air mixing ratio values 1) where differences exceed the expected error level of satellite value and 2) according to the density of ship measurements available. The following formula was finally adopted:

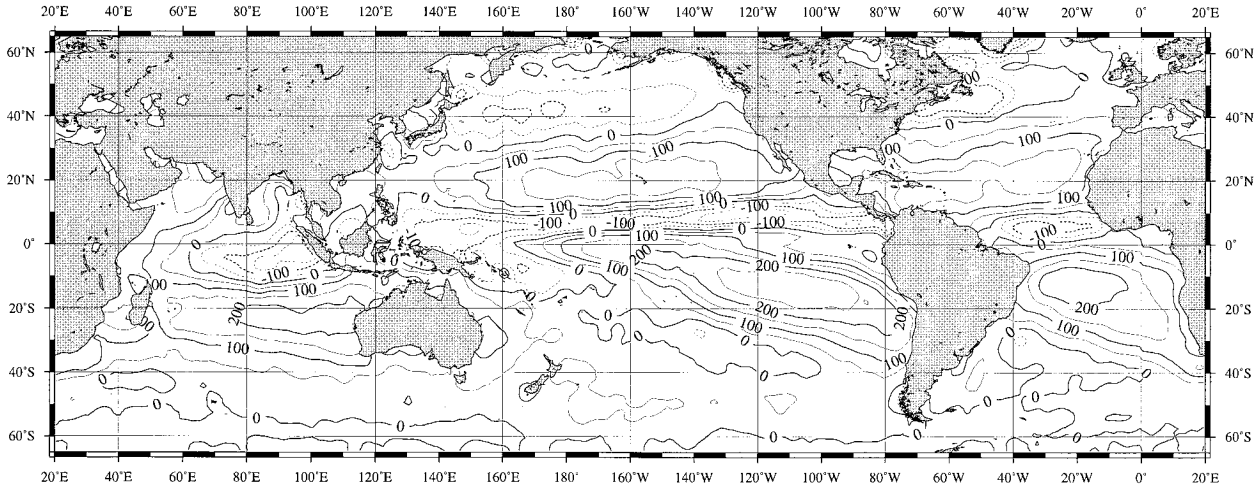

FIG. 1. Three-year averaged satellite-derived evaporation minus precipitation map.

$$Q_a^{\text{blended}} = \left(1 - \frac{1}{\sqrt{N_{\text{obs}}}}\right) Q_a^{\text{ship}} + \left(\frac{1}{\sqrt{N_{\text{obs}}}}\right) Q_a^{\text{satellite}}, \quad (4)$$

where Q_a is the air mixing ratio and $N_{\text{obs}} \geq 1$ is the number of observations that were used to compute the ship air mixing ratio value. The $N_{\text{obs}}^{-1/2}$ shape of the coefficients is in agreement with the dependence of the standard error of the ship-based data on the measurements density (Morissey 1990). Using the new values for the air mixing ratio, the global error of the ship-satellite blended LHF was assessed to be slightly smaller than 30 W m^{-2} (Jourdan and Gautier 1995). For this study, we have used the monthly blended LHF maps between 70°N and 70°S from January 1988 to December 1990 with 1° × 1° resolution to derive the evaporation component of the FWB.

2) PRECIPITATION DATA

The precipitation fields that we used are retrieved from Special Sensor Microwave/Imager (SSM/I) radiometer measurements (Wilheit et al. 1991). The algorithm is based on an iterative process that fits the parameters of a probability distribution function of rainfall intensity to the actual histogram of a combination of brightness temperatures measured in two different channels. The probability distribution function is a lognormal distribution, and the two combined SSM/I channels operate in the microwave domain at 19 and 22 GHz.

Other remote sensed techniques use satellite infrared measurements to estimate rain amount. They are based on the correlation observed between rain rate and high cloud amount. Basically, the fraction of IR brightness temperature below a selected threshold in the histograms of cloud-top temperatures gives an estimate of the high cloud amount. The high cloud amount is then multiplied by a constant rain rate to provide rain amount (Arkin 1979). Janowiak and Arkin (1991) applied the technique to geostationary satellite data and produced the (GOES)[1] Precipitation Index (GPI).

Endly, climatologies (Baumgartner and Reichel 1975; Dorman and Bourke 1981) use ground measurements recorded by coastal gauges and meteorological stations fitted to ship present weather reports and interpolated across the oceans.

The three types of rainfall estimates have been compared by Chiu et al. (1993). The comparison showed that SSM/I annual and seasonal zonal-mean rain rates are larger than climatological estimates but smaller than those estimated from GPI. This general result remains valid in the regions where GPI is known to overestimate. Microwave technique also appeared as a good rainfall estimator for higher latitude. These conclusions, although GPI has an advantage in terms of sampling, led us to use the precipitation estimates computed from SSM/I measurements with Wilheit et al. (1991) algorithm.

3) EVAPORATION MINUS PRECIPITATION

SSM/I global monthly mean precipitation maps are available on a 2.5° × 2.5° grid between 65°N and 65°S. Before computing $E - P$, precipitation fields have been regridded to the evaporation fields' resolution by setting the closest 1° × 1° gridpoint values equal to the appropriate 2.5° × 2.5°mesh value. The difference $E - P$ is then computed for each month separately and averaged in time. Figure 1 is the 3-year (1988–90) averaged $E - P$ map. It shows the expected spatial distribution with positive areas (excess of evaporation) in the tropical and subtropical region and negative areas associated with the equatorial convergence zones and the warm pool

[1] Geostationary Operational Environmental Satellite

region. The other important feature is the maximum located in the southeastern Pacific Ocean.

b. Freshwater transport computation

The appropriate runoff computed by BR is subtracted to the zonally averaged value of $E - P$. The result is integrated from the northern boundary in each ocean to compute the FWT in Eq. (3).

A value of the FWT is required to start the integration. The easiest configuration would be if the oceanic basin was bounded in the north. In this case, the value of FWT at this boundary is zero, but actually none of the oceans fulfill rigorously this condition. The Indian Ocean, although it is closed by a continental boundary at the north, has an incoming flow from the Pacific Ocean through the Indonesian straits, while the Atlantic and the Pacific Oceans are linked through the Arctic Ocean.

The Bering Strait is yet a good candidate to start the integration since it is a bottleneck through which the water has to flow when leaving the North Pacific. Based on the salinity contrast between the Bering Strait and North Atlantic water, BR computed no, or at most negligible, freshwater flux, 0.1 Sv (1 Sv $\equiv 10^6$ m^3 s^{-1}), leaving the Pacific Ocean. Wijffels et al. (1992) demonstrated that this method based on salinity contrast is meaningless for a global study but that pure water fraction of the total oceanic transport must be used. From the 0.8 Sv mass transport reported by Coachman and Aagaard (1988), authors calculated that FWT through the Bering Strait amounts to 0.774 Sv.

For the present computation, this value is used as the starting integration constant along with satellite-derived $E - P$ to compute FWT across southernmost sections. However, our estimate of $E - P$ is only available below 65°N. In the Pacific, it encompasses the Bering Strait and allows to perform FWT computation exclusively with satellite values, but in the Atlantic other values of $E - P$ had to be used at higher latitudes. First, BR's values were used to compute the northernmost contribution, namely, the contribution of the Arctic Ocean to the Atlantic FWT at 70°N. Southward from that point, between 70° and 65°N, the more recent values by Schmitt et al. (1989) were used. In the Indian Ocean the FWT was set equal to zero at 30°N despite the Pacific to Indian throughflow (see Wijffels et al. 1992 for discussion). Southward, integration was stopped at 35°S in the Indian and the Atlantic Oceans while it was done down to 45°S in the Pacific.

3. Results

a. Evaporation minus precipitation

The monthly map of $E - P$ for May 1988 is first compared to the corresponding analyzed output field of the European Centre for Medium-Range Weather Forecasts (ECMWF) Global Circulation Model (GCM). Both $E - P$ fields are presented with the same spatial coverage at the same resolution (Fig. 2).

A fairly good agreement is observed between both maps. The limits between precipitative and evaporative regions are consistent and the magnitude of the extrema agree within 2 mm day^{-1}. Systematic differences are observed in the location of some evaporative regions: in the Indian and North Atlantic Oceans, maxima of evaporation are centered farther west on our map than on the model output. The best agreement is achieved in the South Atlantic Ocean where structures compare well in extension and magnitude. Results over the precipitative regions also agree rather well in the equatorial Atlantic and Pacific but exhibit up to a -4 mm day^{-1} difference in the northwestern Pacific. In the southeastern Pacific, while both maps suggest a similar maximum centered around 15°S, 90°W, it is found to spread out farther west with larger magnitude in the satellite data. Satellite data also show a minimum slightly farther west and south, which is not apparent on the GCM's map.

In order to have more quantitative insight, the next step was to validate the results with respect to existing climatology of $E - P$. Schmitt et al. (1989) computed global annual as well as monthly $E - P$ maps over the North Atlantic by subtracting precipitation data of Dorman and Bourke (1981) to Bunker's evaporation climatology (Bunker 1976).

Figure 3 shows the climatology (upper panel), the 3-year averaged satellite-derived map (middle panel) and their difference map (lower panel). The difference exhibits coherent features that correlate with $E - P$ patterns: positive differences (larger satellite $E - P$ values) are found over regions where evaporation dominates and negative differences over precipitation areas. The largest positive difference (150 cm yr^{-1}) is observed in the southeastern tropical Pacific, whereas northwestern parts of the subtropical basins in the Northern Hemisphere and eastern equatorial regions experience the highest negative values (-100 cm yr^{-1}). Overall, our results enhance the climatology distribution and differences are normally distributed with 36.7 cm yr^{-1} rms. Enhancement is not surprising since present computation is based on 3 years of satellite data when the climatology includes several decades of marine reports.

A noticeable consequence of this new $E - P$ computation is the absence of the Gulf Stream signature in the North Atlantic Ocean. The Gulf Stream is rather well marked in the evaporation field, but large precipitation (around -250 cm yr^{-1}) over the northwestern part of the basin (30°–60°N, west of 40°W) compensates for the evaporation and strongly dominates off Newfoundland, creating up to -150 cm yr^{-1} disagreement with the climatology.

A more thorough comparison has been performed on a seasonal basis in the North Atlantic. Difference maps (Fig. 4) confirm that the largest disagreement (up to

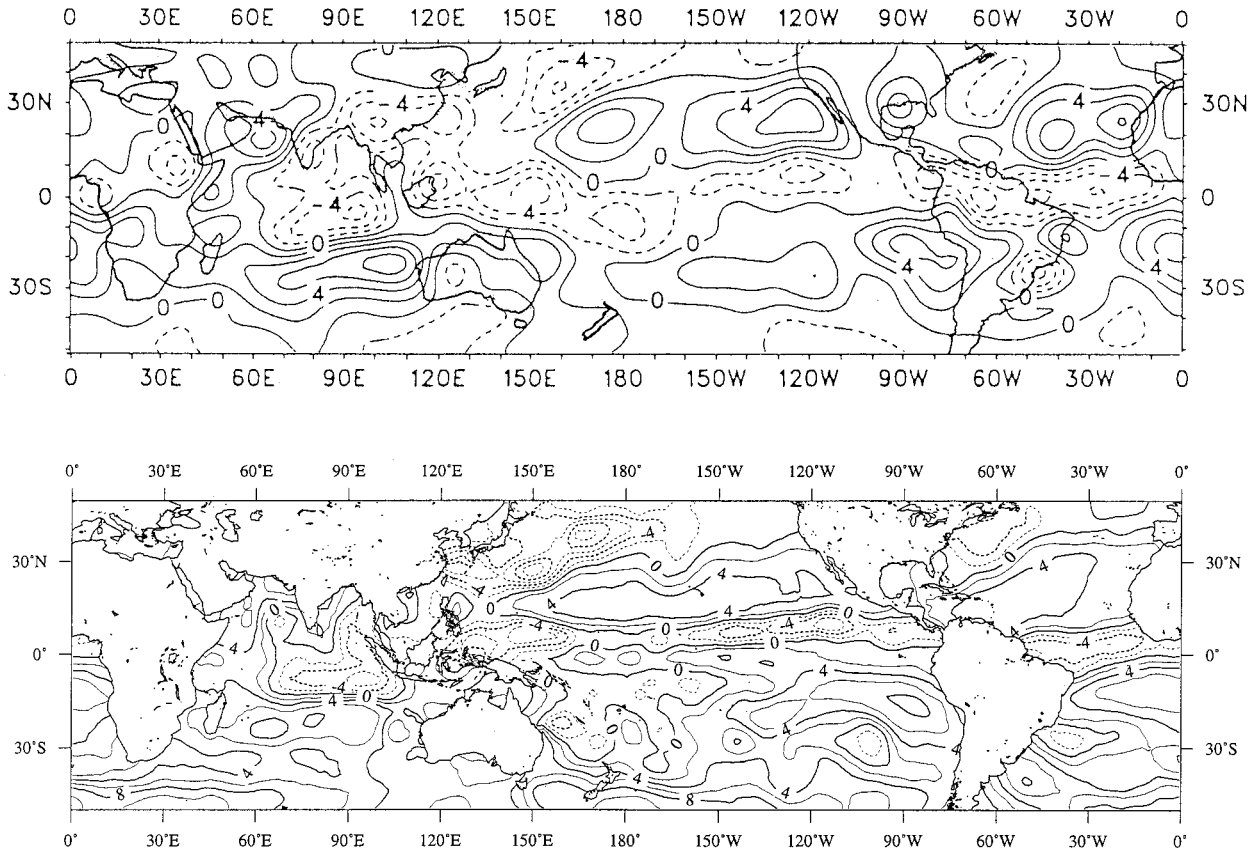

FIG. 2. Monthly evaporation minus precipitation map for May 1988. The top panel shows ECMWF analyzed field (from Trenberth 1991); bottom panel shows the results of the present study.

-275 cm yr^{-1}) is experienced during the winter season. At that time of the year $E - P$ estimates disagree on the leading process: Climatology shows net loss of freshwater, whereas satellite field indicates a net gain of freshwater. In the subtropics, differences are positive and reach 125 cm yr^{-1} in winter.

However, it is interesting to note that, if local values of $E - P$ can strongly differ, seasonal cycles agree in magnitude and spatial distribution. Figure 5 is the plot of the monthly averaged satellite $E - P$ values (solid line with triangles) and corresponding climatological average (solid line with diamonds). The gap between both curves is around 15 cm yr^{-1} and quite constant throughout the year except from June to September. The most striking difference (25 cm yr^{-1}) shows up in August and September when monthly average climatology strongly increases. This peak surprisingly makes the climatology seasonal cycle less smooth than the satellite-derived one. Spatial features are preserved accordingly: between winter and spring season $E - P$ rate decreases by around 50 cm yr^{-1} in the eastern part of the Atlantic and 100 cm yr^{-1} over the Gulf Stream. The seasonal variability of the intertropical convergence zone region is also reproduced by satellite-derived $E - P$ maps with consistent amplitude and displacement as shown on Fig. 4 by the northward shift of the band of negative values toward the Northern Hemisphere with a constant magnitude.

b. Freshwater transport

The results of the FWT transports are presented on the Figs. 6a–c. For comparison purposes, we have plotted the Wijffels et al. (1992) results (dashed curve) and the available values from oceanographic computations adjusted by the proper integration constant. The third curve on the first panel is the Schmitt et al. (1989) FWT, also adjusted by the same constant.

We clearly distinguish 1) the regions where all the computations agree, like in the Atlantic Ocean and north of 25°N in the Pacific; 2) the regions where the computations based on the air–sea exchange budget fairly agree but differ from the oceanographic estimates, like in the Indian Ocean; and 3) the regions where the computations based on the same method strongly disagree, like south of 15°N in the Pacific Ocean.

In the Atlantic, the transport is directed southward everywhere and becomes smaller from north to south. Superimposed to this general trend, one observes variations related with ocean–atmosphere exchanges. South-

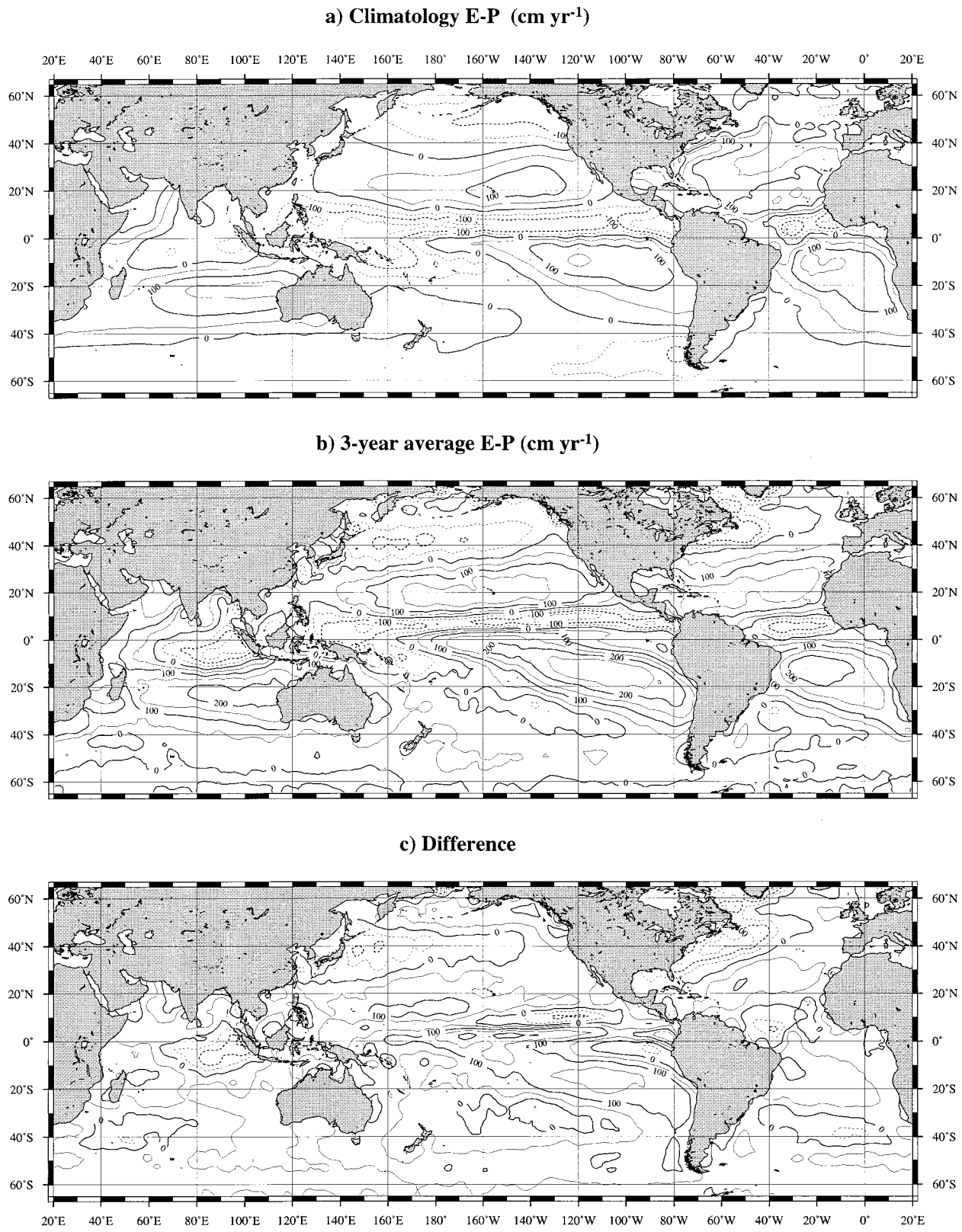

FIG. 3. Global multiyear-averaged evaporation minus precipitation maps as computed with (a) climatological *E* and *P* fields, (b) satellite-derived *E* and *P* fields (same as in Fig. 1). Panel (c) shows the difference between both estimates (b − a). Isopleths are separated by 50 cm yr^{-1}.

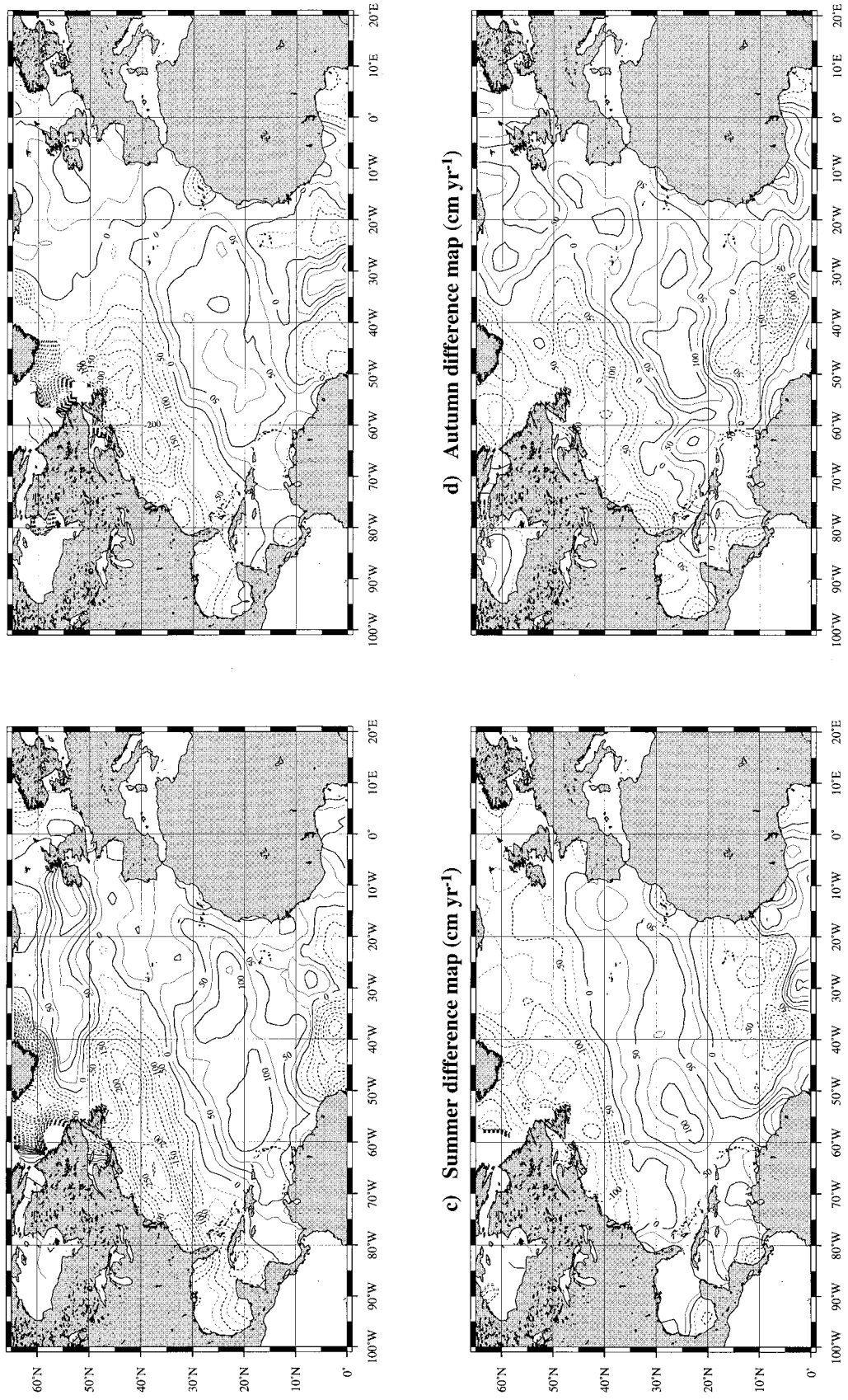

FIG. 4. Difference maps between multiyear seasonally averaged satellite-derived and climatological $E-P$ fields over the North Atlantic Ocean for (a) winter season (Dec–Feb), (b) spring season (Mar–May), (c) summer season (Jun–Aug), and (d) autumn season (Sep–Nov). Isopleths are separated by 25 cm yr^{-1}.

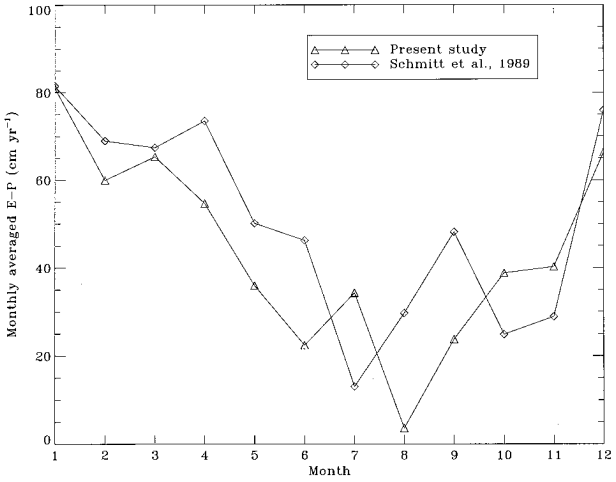

FIG. 5. Multiyear monthly averaged satellite-derived (triangles) and climatological (diamonds) $E-P$ values.

ward transport is first enhanced down to 40°N then decreases between 40° and 10°N while remaining negative, showing that freshwater import from the Arctic Ocean and freshwater gain at high latitudes compensate for the evaporation in the tropical regions. Again southward, FWT increases between 10°N and 5°S when the excess of freshwater combines with the ITCZ net gain. The resulting amount of water keeps flowing southward and balances the loss of water in the southern Atlantic Ocean. At 35°S the FWT value is only very slightly negative and equals −0.07 Sv.

Present FWT values differ from climatology-based estimates at the most by 0.22 Sv around 30°N. At 35°S, where the difference is expected to be the largest because of the cumulative propagation of the errors throughout the integration (gray-shaded band), the difference is 0.11 Sv. Both curves start to disagree at 40°N because of the strong precipitation area found in our results (Figs. 3 and 4) that contributes to freshwater gain by the ocean that intensifies southward FWT. On the contrary, the budget is balanced in climatology-based results and southward FWT remains constant. This bias becomes more pronounced between 35° and 25°N when the Gulf Stream positive contribution reduces climatological FWT whereas it does not contribute to our results. Farther south, this discrepancy decreases because of larger evaporation rate and finally satellite-derived FWT exceeds climatological estimates in the southern Atlantic.

FWT transport in the Pacific Ocean is directed northward everywhere but relative variations roughly follow the same pattern as in the Atlantic. According to the present results, the outflow of freshwater through the northernmost boundary of the Pacific Ocean requires a northward inflow of 2.48 Sv at 45°S. A large part (72%) is lost between 5° and 45°S because of the strong evaporation that takes place in the southeastern tropical region, and only 0.74 Sv finally crosses the equator. Between 0° and 10°N, strong precipitation within the ITCZ region supplements the northward flow of freshwater crossing the equator and compensates for the evaporation that takes between 10° and 35°N. Farther north, ocean gains water from the atmosphere and transfers the required 0.774 Sv of freshwater to the Arctic Ocean.

When compared to other estimates, the agreement is rather good north of 20°N especially with direct measurements. The largest difference (−0.09 Sv) is observed at 30°N with respect to the Wijffels et al. (1992) computation. Differences with Roemmich and McCallister (1989) estimates are smaller: at 24° and 47°N both values are identical and at 35°N all three computations agree within 0.1 Sv. South of 15°N, however, both curves differ drastically in magnitude. Wijffels et al. (1992) results show no or negligible transport through the equator and a small northward FWT of 0.26 Sv at 45°S, whereas our computation implies a one order magnitude larger net import (2.48 Sv) from the Antarctic Circumpolar Current (ACC).

Better overall agreement between exchange-budget-based computations is obtained in the Indian Ocean. According to the present results, the FWB is locally balanced up to 19°N. Farther south, it first loses water up to 5°N then gains water south of it, inducing a northward FWT between 20°N and 10°S. At 10°S the FWT is close to zero (0.04 Sv) indicating that north of that latitude the ocean is in balance. In its southern part, the Indian Ocean loses a large amount of water and at the southern boundary the difference from Wijffel's value is 0.35 Sv. In this part of the global ocean none of the results are comparable with direct estimates available (Fu 1986; Toole and Raymer 1985). The smallest deviation, observed at 18°S with respect to Toole and Raymer's (1985) value, amounts to 0.3 Sv.

4. Discussion

Except in the Southern Pacific, the agreement between the results is encouraging, considering some of the problems inherent to the computation method and the nature of the dataset. Assuming a simple square combination of the blended evaporation rms error, one finds that the maximum FWT error, as result of the meridional integration over 100°, ranges from 0.45 to 1.83 Sv rms (gray-shaded areas in Fig. 6). The comparison with Wijffels et al's. (1992) results in the Atlantic, Indian and North Pacific Oceans shows that the error level is more likely around 0.2 Sv rms, and it is not clear which computation contributes most to this difference.

Indeed, the error level provided by BR for the FWB components is estimated with respect to the atlases they have based their computation on. It shows, however, that the precipitation and evaporation are the less accurate components. Since, more complete evaluation of datasets based on marine reports have been performed. Isemer and Hasse (1991) showed that the relation used

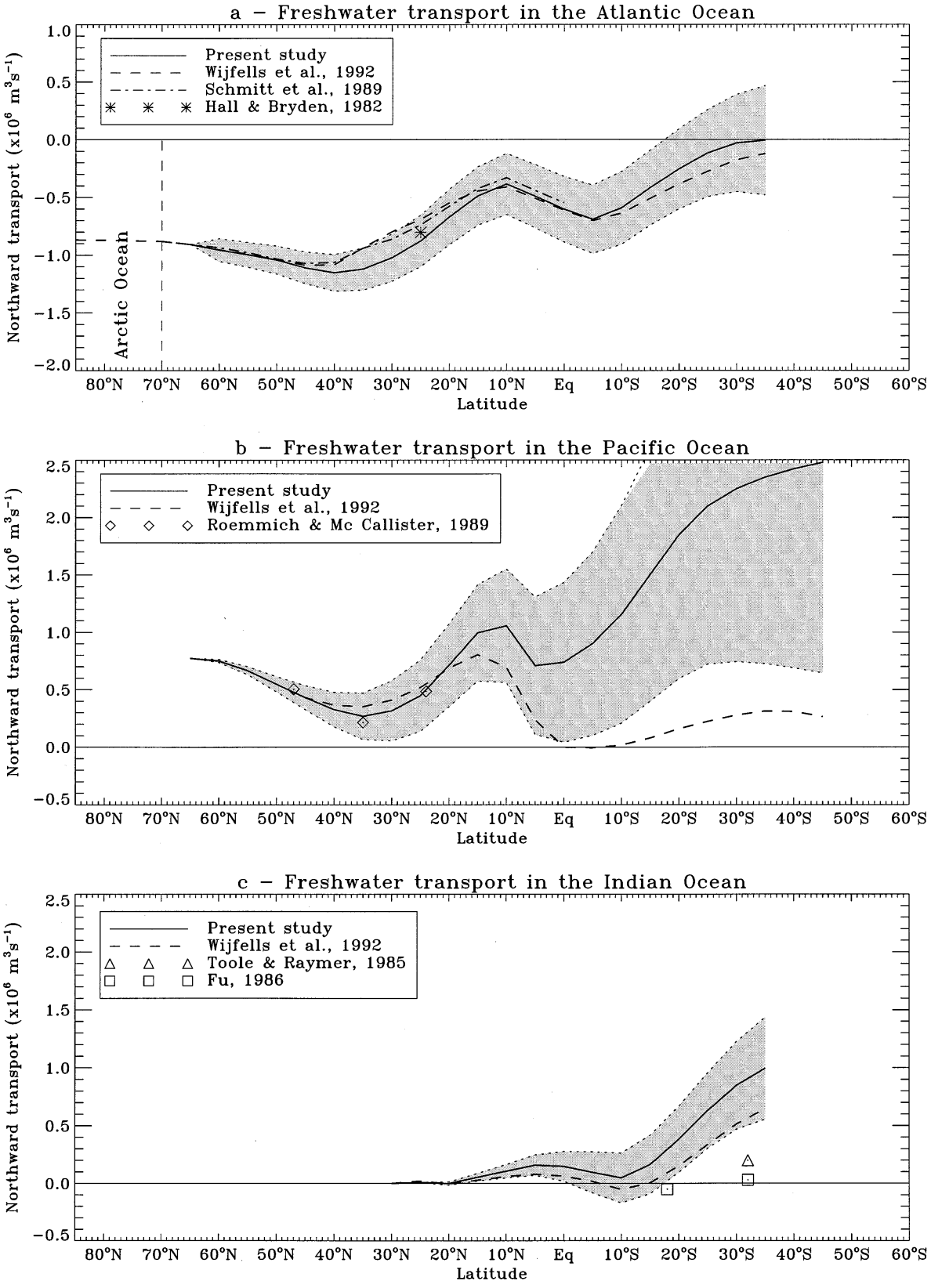

FIG. 6. Freshwater transport estimates for the Atlantic, Pacific, and Indian Ocean.

to convert the Beaufort scale estimates into physical quantities affects the assessment of the wind speed. This mainly concerns the pre–World War II reports that were made by a visual estimate of the sea state according to the Beaufort scale. Authors found that the corresponding underestimation in the monthly mean evaporation reaches up to 40 W m^{-2} between 0° and 40°N in the Atlantic, which corresponds to an overestimation by 50 cm yr^{-1} in the FWB. The datasets used by BR to build their atlas contain a majority of these reports, and neither Schmitt et al. (1989) or Wijfells et al. (1992) could use the revised version of the Bunker's atlas produced by Isemer and Hasse. Although the magnitude of the corrections is now considered to be excessive, this error is likely to contribute to the differences observed in $E - P$ seasonal maps and FWT curves.

Finally, it should also be remembered that our computation is based on 3 years whereas the climatologies include several decades of marine reports. Therefore, as expected, our results show stronger gradients and larger extrema than the climatology.

In the southern Pacific Ocean, inconsistency between FWT estimates exceeds error level too excessively to be justified by the previous explanations. The major concern is the northward transport at 45°S, which is 10 times larger than previous values and indicates that the Pacific as a whole, mainly because of the process in the southeastern Pacific, is an evaporative basin. Comparison with climatology (Fig. 3) shows that $E - P$ differ by more than 150 cm yr^{-1} over this region and that it results from an area of high net evaporation excess, centered at 15°S, 110°W covering a large part of the southeastern Pacific. Therefore, it is questionable whether our blended evaporation field is overestimated. Validation of E and P fields is very difficult in this part of the ocean, which has the poorest spatial coverage of ship and in situ data of the global ocean. For the same reasons, no oceanographic computations of the FWT are available at the southern boundary of the Pacific with which we can compare our results. The only way to validate results in these regions would be now to compare them more thoroughly with atmospheric and oceanic GCM results, as well as to study the consequences on the global circulation scheme.

Considering the limitations affecting the BR computation along with the satisfactory agreement of the results outside the southern Pacific Ocean, we think the present computation is representative of the air–sea exchange and the oceanic FWT. Also, strong transport directed northward in the South Pacific appears as the effect of an atmospheric feature that, so far, had not been properly sampled. We certainly cannot confirm the magnitude of the FWT in this region, but it is reasonable to think that the South Pacific imports freshwater from the ACC.

5. Conclusions

Satellite-derived evaporation and precipitation fields have been used to compute global 3-year averaged maps of $E - P$. After combining with the appropriate value of the runoff, the values of the FWB are integrated southward to compute the FWT in each ocean.

On a monthly basis and with respect to ECMWF output, monthly $E - P$ maps compare within 2 mm day^{-1}. Comparisons with results based on climatological atlases show that long-term global agreement is 36 cm yr^{-1} rms and that the seasonal cycle, at least over the North Atlantic Ocean, is consistent in magnitude within 15 cm yr^{-1}. Local differences, however, may be much larger, indicating that satellite-derived results enhance climatological features leading to larger extrema and stronger gradients. In the northwestern part of the Atlantic Ocean, for instance, the satellite FWB is largely dominated by precipitation. A consequence is the absence of the Gulf Stream signature in the $E - P$ maps and no contribution to the FWT. Largest differences are found over the southern Pacific where in situ measurements sampling is poor.

Difference in FWT at the southernmost boundary of the basins is 0.11 Sv in the Atlantic and 0.35 Sv in the Indian Ocean. Overall, the error level is estimated to be 0.2 Sv rms. This level of error along with the sampling deficiency of the climatological dataset in the Southern Hemisphere gives us confidence that the South Pacific Ocean is transferring freshwater to the atmosphere and needs to import freshwater from the Southern Ocean. The amount of freshwater that enters in southern Pacific Ocean, however, differs by a factor of 10 from the climatological estimate. Present FWT value is likely overestimated to satisfy the global freshwater cycle (Chen et al. 1994) but shows there is agreement on the matter that freshwater may enter the southern Pacific Ocean, even if the magnitude of the transport is still an issue.

Acknowledgments. This study has been made possible by a grant from National Aeronautics and Space Administration (NASA Grant NAGW-2460). The authors wish to thank Dr. Al Chang (NASA/Goddard Space Flight Center) for providing us with precipitation dataset, Dr. R. Schmitt (WHOI) for the $E - P$ climatology and fruitful contacts, and reviewers whose comments considerably helped improving the manuscript.

REFERENCES

Arkin, P. A., 1979: The relationship between fractional coverage of high cloud and rainfall accumulations during GATE over the B-scale array. *Mon. Wea. Rev.,* **107,** 1382–1387.

Baumgartner, A., and E. Reichel, 1975: *The World Water Balance.* Elsevier, 179 pp.

Bunker, A. F., 1976: Computation of energy flux and annual air–sea interaction cycles of the North Atlantic Ocean. *Mon. Wea. Rev.,* **104,** 1122–1140.

Cardone, V. J., J. G. Greenwood, and M. A. Cane, 1990: On trends in historical marine wind data. *J. Climate,* **3,** 113–127.

Chen, T.-C., J. Pfaendtner, and S. P. Weng, 1994: Aspects of the hydrological cycle of the ocean–atmosphere system. *J. Phys. Oceanogr.,* **24,** 1827–1833.

Chiu, L. S., A. T. C. Chang, and J. Janowiak, 1993: Comparison of

monthly rain rates derived from GPI and SSM/I using probability distribution functions. *J. Appl. Meteor.,* **32,** 323–334.

Coachman, L. K., and K. Aagaard, 1988: Transport through Bering strait: Annual and interannual variability. *J. Geophys. Res.,* **93,** 15 535–15 539.

Dorman, C. E., and R. H. Bourke, 1981: Precipitation over the Atlantic Ocean, 30°S to 70°N. *Mon. Wea. Rev.,* **109,** 554–563.

Esbensen, S. K., D. B. Chelton, D. Vickers, and J. Sun, 1993: An analysis of errors in Special Sensor Microwave Imager evaporation estimates over the global oceans. *J. Geophys. Res.,* **98,** 7081–7101.

Fu, L. L., 1986: Mass, heat, and freshwater fluxes in the South Indian Ocean. *J. Phys. Oceanogr.,* **16,** 1683–1693.

Hall, M. M., and H. L. Bryden, 1982: Direct estimates and mechanisms of ocean heat transport. *Deep-Sea Res.,* **29,** 339–359.

Hellerman, S., and M. Rosenstein, 1983: Normal monthly wind stress over the world ocean with error estimates. *J. Phys. Oceanogr.,* **13,** 1093–1104.

Isemer, H.-J., and L. Hasse, 1991: The scientific Beaufort equivalent scale: Effects on wind statistics and climatological air–sea estimates in the North Atlantic Ocean. *J. Climate,* **4,** 819–836.

Janowiak, J., and P. A. Arkin, 1991: Rainfall variations in tropics during 1986–1989 as estimated from observations of cloud-top temperature. *J. Geophys. Res.,* **96** (Suppl.), 3359–3373.

Jourdan, D., and C. Gautier, 1995: Comparison between global latent heat flux computed from multisensor (SSM/I and AVHRR) and from in situ data. *J. Atmos. Oceanic Technol.,* **12,** 46–72.

Leetma, A., and A. Bunker, 1978: Updated charts of the mean annual wind stress convergences in the Ekman layers, and Sverdrup transport in the North Atlantic. *J. Mar. Res.,* **36,** 311–322.

Morissey, M. L., 1990: An evaluation of ship data in the equatorial western Pacific. *J. Climate,* **3,** 99–112.

Roemmich, D., and T. McCallister, 1989: Large scale circulation of the North Pacific Ocean. *Progress in Oceanography,* Vol. 22. Pergamon, 171–204.

Schmitt, R. W., P. S. Bogden, and C. V. Dorman, 1989: Evaporation minus precipitation fluxes in the North Atlantic. *J. Phys. Oceanogr.,* **19,** 1208–1221.

Taylor, P. K., 1984: The determination of surface fluxes of heat and water by satellite microwave radiometry and *in situ* measurements. *Large Scale Oceanographic Experiments and Satellites,* C. Gautier and M. Fieux, Eds., Reidel, 288 pp.

Toole, J. M., and M. E. Raymer, 1985: Heat and freshwater budgets of the Indian Ocean—Revisited. *Deep-Sea Res.,* **32,** 917–928.

Trenberth, K. E., 1991: Climate diagnostics from global analyses: Conservation of mass in ECMWF analyses. *J. Climate,* **4,** 707–722.

Wijffels, S. E., R. W. Schmitt, H. L. Bryden, and A. Stigebrandt, 1992: Transport of freshwater by the oceans. *J. Phys. Oceanogr.,* **22,** 155–162.

Wilheit, T. T., A. T. C. Chang, and L. S. Chiu, 1991: Retrieval of monthly rainfall indices from microwave radiometric measurements using probability density functions. *J. Atmos. Oceanic Technol.,* **8,** 118–136.